

Fast response infrared photodetector based on reduced graphene oxide

H. AHMAD^{a,b,*}, M. TAJDIDZADEH^a, M. F. ISMAIL^a, T. M. K. THANDAVAN^a

^aPhotonic Research Center, University of Malaya, 50603 Kuala Lumpur, Malaysia

^bPhysics Dept., Faculty of Science, University of Malaya, 50603 Kuala Lumpur, Malaysia

A fast-response-infrared-reduced graphene oxide (rGO) photodetector was prepared via drop casting. A silver (Ag) source and 50 nm-thick drain electrodes were deposited to obtain an active channel of 5 mm x 2 mm dimension. The Schottky contacts among the rGO semiconducting layer, Ag source, and drain electrodes enabled the efficient transfer of photo-generated charge carriers. The photodetector showed high sensitivity toward a laser illumination wavelength of 974 nm. Current–voltage characteristics showed low sensitivity in the negative bias region, but a significantly high response was attained at increased laser power levels. Photoresponsivity and external quantum efficiency (EQE) were determined at different laser power levels ranging from 7.64 mW to 121.70 mW. The highest EQE was obtained at the lowest laser power level of 7.64 mW. Fast response and recovery time were achieved at 4.01 and 96.28 μ s, respectively, at laser frequency modulation of 5000 Hz, although the photoresponsivity remains low.

(Received September 13, 2017; accepted April 9, 2020)

Keywords: Infrared photodetectors, Reduce graphene oxide, Drop casting

1. Introduction

Comprising a single layer of carbon atoms in a hexagonal honeycomb lattice, graphene is considered a promising 2D material in the current era. Graphene is attracting great interest because of its notable properties, such as fast electron mobility, high surface area, high Fermi velocity, and linear energy dispersion relation [1]. Owing to these properties, graphene is widely used in various fields, such as sensor, electronics, and catalysis [2, 3]. Immediately after its discovery, graphene was already observed to display unique photonic properties. It can absorb a number of photons from the visible to infrared (IR) range. This observation has been the basis for the development of detectors and sensing devices based on graphene [4-8] with a single atomic layer [9, 10]. Further extensive works on graphene revealed graphene oxide (GO) as another promising candidate material for ultra-broadband photodetection. Both materials have attracted considerable attention from researchers developing photodevices [11, 12]. For example, Liu et al. and Mak et al. determined that the absorption spectra of graphene and GO-based photodetectors could cover the entire ultraviolet (UV) and IR ranges [4, 13]. Meanwhile, preparation of graphene and GO in thin layers has been one of the most emphasized works aimed at investigating the remarkable properties of these materials. Xia et al. structured graphene field-effect transistors (FETs) by using a single or few layers of graphene sheets to produce an ultrafast photodetector [8].

The photoresponsivity of the ultrafast photodetector did not degrade at optical intensity modulations of up to 40 GHz and intrinsic bandwidth of up to 500 GHz. Good conductive [14,15] reduced GO (rGO) can be obtained via

graphite oxide reduction [16-17]. rGO can be deposited as significantly conductive thin films onto a large variety of substrates [19, 20] and is believed to be a promising 2D material for large-area electronics [21], highly sensitive gas sensors [22], and photocatalytic technologies [23-27]. Nevertheless, an ideal photodetector allows zero bias operation in a wide and selectively detected spectrum. Fast response and recovery time [28, 29], as well as high sensitivity, at low laser power are some of the important factors to be investigated. Some investigations have been mainly focused on IR photoresponsivity behavior, but studies on photoresponsivity properties in the visible and near IR regions are endless, however not many photodetectors related to far IR regions greater than 1500 nm have been investigated. A novel photodetector device featuring a hybrid rGO/p-type silicon structure with a built-in electric field is required to achieve such a goal. For rapid and efficient separation of photogenerated charge carriers, the electric field should exist at the interface between certain hybrid materials that provides a driving force [30, 31]. High photoresponsivity in the visible range was identified by Darbari et al. from a hybrid rGO/zinc oxide (ZnO) nanostructured photodetector [32]. Zhang et al. [33] also worked on hybrid UV photodetector based on ZnO and poly (N-vinylcarbazole) (PVK) materials. The photodetector showed high photoresponsivity because of the efficient carrier separation and convenient charge transport between ZnO and PVK [33]. Fernandes et al. outlined that rGO/p-Si heterojunction photodetector elicited the transition between direct tunneling and field emission because of the formation of a broken gap at the junction [34]. They also suggested that mid-IR response was elicited by the excitation of minority charge carriers from the p-Si to the

rGO layer. Chang et al. and Acik et al. found that defects related to oxygen in the rGO can remarkably enhance the absorption of near-IR illumination because of electron–phonon coupling [35, 36].

In this study, rGO was prepared on silicon dioxide (SiO_2)/p-Si substrate via simple drop casting. High photoresponsivity and fast response toward IR light was described in light of new information to a promising direction for fabricating self-powered photodetectors.

2. Experiments

Fig. 1 illustrates the schematic design of a fabricated photodetector based on rGO on SiO_2 /p-Si substrate. A homemade stainless-steel mask was placed on the SiO_2 /p-Si substrate to allow the formation of $5 \times 2 \text{ mm}^2$ channel for rGO and $5 \times 5 \text{ mm}^2$ channel for the Ag electrodes. The rGO solution was drop casted on the top of the SiO_2 layer to fill the photodetector channel length and width of 5 and 2 mm, respectively. The solution was also spread partially onto a portion of the channel to form the Ag electrodes. The SiO_2 /p-Si substrate was then dried in a desiccator for 24 h to form a good contact with the substrate.

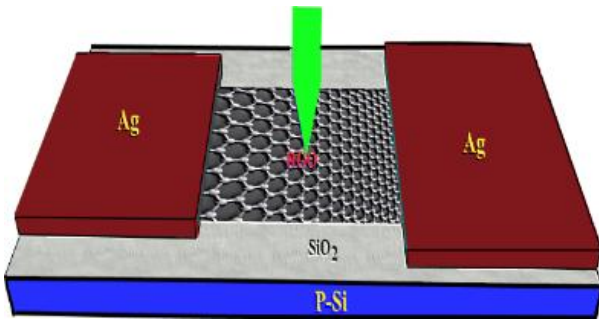


Fig. 1. Schematic diagram of prepared IR reduced graphene oxide photodetector under the illumination of laser at 974 nm (color online)

The substrate containing the dried rGO channel was placed in a DC sputtering machine to deposit source and drain contacts of Ag. Prior to the deposition of Ag electrodes, the $5 \text{ mm} \times 2 \text{ mm}$ rGO channel was covered with a thin stainless-steel metal sheet. A Schottky contact formed between the Ag and rGO [37, 38]. The homemade stainless-steel mask was removed from the SiO_2 /p-Si substrate, and the thickness of the Ag electrodes was measured using VeecoDekTak 150. The structural property of graphene was examined using a Renishaw in-Via Raman Spectrometer. The Quanta 450 FEG scanning electron microscopy (SEM) was performed to investigate surface morphology of the photodetector, and energy-dispersive X-ray spectroscopy (EDX, X-Max Series) was used for elemental analysis.

Laser illumination at a wavelength of 974 nm was achieved using a cooled butterfly laser diode (LD; LC96A74P – 20R), which was mounted to LD controller (CLD1015). The laser source was placed at a fixed

distance of 10 mm from the photodetector to illuminate and cover the active area. The current–voltage (I - V) characteristics were collected using a Keithley 2410 Source Meter unit for voltage range from -15 V to $+15 \text{ V}$. The laser power varied as a function of the LD current. Laser power levels of 0, 7.64, 36.21, 64.70, 93.25, and 121.70 mW were obtained from the corresponding LD currents of 0, 50, 100, 150, 200, and 250 mA, respectively. Frequency modulation was achieved using a 30 MHz Synthesized Function Generator (DS345), which was connected to the LD pump controller. The frequency responses were recorded as the modulation frequency tuned at various frequencies from 1 Hz to 5000 Hz by utilizing an oscilloscope (YOKOGAWA DLM2054 Mixed Signal) unit.

3. Results and discussions

3.1. SEM and EDX results

The obtained SEM image as in Fig. 2(a) reveals the distribution of rGO flakes on the SiO_2 /p-Si substrate [39]. Tiny micro sheets are observed in the rGO flakes, which are randomly scattered over that substrate. The EDX and elemental mapping results are evident, as shown in Fig. 2(b). Fig. 2(b) depicts the elemental composition in the rGO photodetector on the SiO_2 /p-Si substrate. The selected area of the corresponding EDX spectrum (Fig. 2(b)) is shown in Fig. 2(c). In the selected image, which consists of rGO and SiO_2 , the weight composition of carbon (C), oxygen (O), and Si are 44.82%, 35.35%, and 19.83%, respectively. This result deliberately signifies that the drop-casted material is rGO because of the lower weight composition of O compared with that of C. Figs. 2(d–f) represent the various well-defined C, Si, and O peaks, which further confirm the presence of the elements in the fabricated photodetectors. The comparison observation between Fig. 2d and 2e signifies profound distribution of C elements on SiO_2 substrate. Meanwhile, Fig. 2f shows uneven distribution of O elements on SiO_2 . It is clearly observable that only a few O elements are bonded with C elements of rGO whereas large number of O elements bonded with Si elements of SiO_2 . Therefore, the detection of O elements together with C elements definitely reveals formation of rGO on SiO_2 substrate.

3.2. Raman Scattering Result

The recorded Raman spectrum on a Renishaw in Via Raman microscope system with 514 nm laser excitation is indicated in Fig. 3. Two strong characteristic bands at 1345 and 1577 cm^{-1} can be assigned to D and G bands. The D band corresponds to the sp^2 structural disorder of carbon, and the G band is attributed to the C–C stretching mode in the graphite lattice represented in the rGO layer [40]. Two other minor bands are observable at 2674 and 2919 cm^{-1} . The band at 2674 cm^{-1} is known as the 2D band, which indicates that the graphene layers are few.

The band is observed to be broadened because of the presence of few layers, which have some defects, on the drop-casted rGO solution on the SiO₂/p-Si substrate. The band at 2919 cm⁻¹ is known as the S3 band, which is a

second-order peak derived from the combination of D and G peaks [41]. The 950 cm⁻¹ peak can be attributed to the second-order Raman scattering effect of silicon [39, 42].

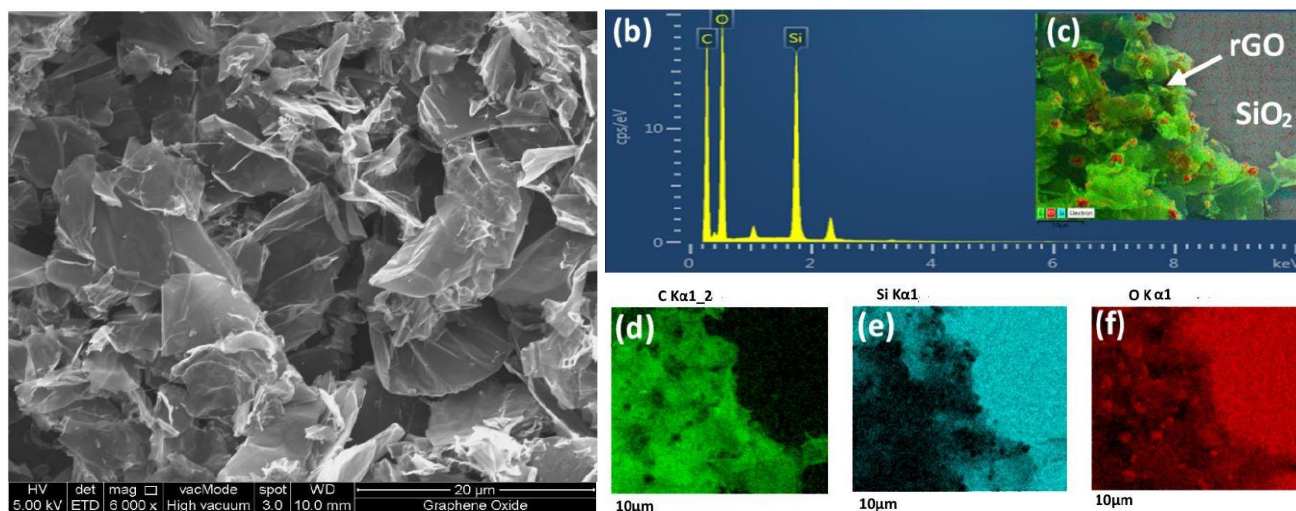


Fig. 2. (a) SEM image rGO, (b) and (c) are the respective EDX results and selected area of rGO layer. (d), (e) and (f) are the respective elemental mapping images of rGO on p-Si for C, O and Si (color online)

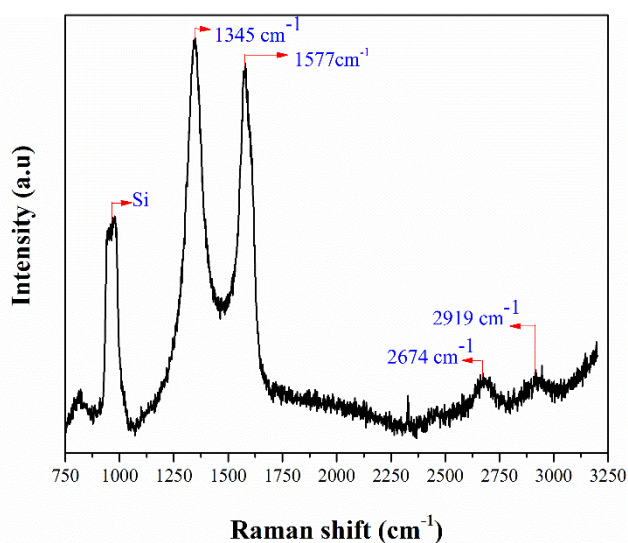


Fig. 3. Raman spectroscopy and (b) SEM image of rGO on SiO₂/p-Si substrate

3.3. I-V Characteristics

The *I-V* characteristics of the fabricated IR rGO photodetector obtained at various laser powers are shown in Fig. 4. The *I-V* curves of the dark current and photocurrent under the illumination of laser power levels of 7.46, 36.21, 64.70, 93.25, and 121.70 mW at a wavelength of 974 nm indicate a rising mode as the DC bias voltage is swept from -15 to +15 V. The photocurrent increases at increased laser power levels. This result further confirms a good Schottky behavior, which is due to

the Fermi level difference between the rGO and Ag electrodes. Fig. 4(b) depicts that the dark current and photocurrent increases at a DC bias voltage around 2.0 V. However, the photocurrent under laser illumination increases drastically to a greater extent than the dark current. The photocurrent seems to be increasing linearly under a DC bias voltage, whereas slight changes are observed at a DC bias voltage of 7.5 V. At this voltage, the generation of photocurrent decreases at all laser power levels, but a profound decrement is observed at low laser power of 7.64 mW. Therefore, the absorption of photons over a wide range of wavelengths from visible to IR by rGO is attainable [9, 10], and the electrical conductivity of IR rGO photodetector increases at various laser power levels. This phenomenon is due to the generation of reduced electron-hole (*e-h*) pairs at laser power of 7.64 mW. Therefore, the limitation in the absorption of light energy also depends on laser power. High photocurrent is measured to be approximately 280 μA at 121.70 mW laser power.

Fig. 4(c) reveals the distribution of photocurrent in reverse DC bias voltages from 0 V to -7.0 V. The *I-V* curve of the laser at 7.64 mW is lower than those at dark current and laser powers of 36.21, 64.70, 93.25, and 121.70 mW. The laser at 7.64 mW exhibits high generation of photocurrent compared with other high laser power levels (36.21, 64.70, 93.25, and 121.70 mW) in the reverse bias region. Thus, the fabricated photodetector is useful for detecting low laser power in the reverse DC bias region and highly sensitive to illumination of high laser power in the forward bias region. As a consequence of the absorption of light, the *e-h* pairs are generated due to the Schottky-like barrier at the metal graphene contact [43,

44] when an external field is applied. The $e-h$ pairs become separated, and a photocurrent is generated. A similar phenomenon can occur in the presence of an internal field formed by photoexcitation [45, 46]. The mobility of insulator (SiO_2) is intrinsically low. Thus, an external voltage is required to separate the photogenerated $e-h$ pairs before they recombine, indicating detector action.

Response time is defined as the time in which the photocurrent increases from 10% to 90% of the peak current, and recovery time is defined in a similar manner. Fig. 5 shows the time-dependent photoresponsivity of IR photodetectors based on rGO under 974 nm laser irradiation at different frequencies. The obtained result implies that photoresponsivity drastically changes with

increasing frequency. Fast response time of 4.01 μs and recovery time of 96.28 μs were obtained at frequency modulation of 5000 Hz. These values are much lower than the other recorded responses and recovery times at 1, 10, 100, and 1000 Hz. The detailed summary of the response and recovery time at different modulation frequencies is shown in Table 1. The decreasing trends of response and recovery time from 11.97 μs to 4.01 μs and from 712.33 μs to 96.23 μs , respectively, is evaluated. These trends correspond to the increased modulation frequencies from 1 Hz to 5000 Hz. The response and recovery time of the device exhibits good reproducibility properties after several different test cycles with light ON and OFF.

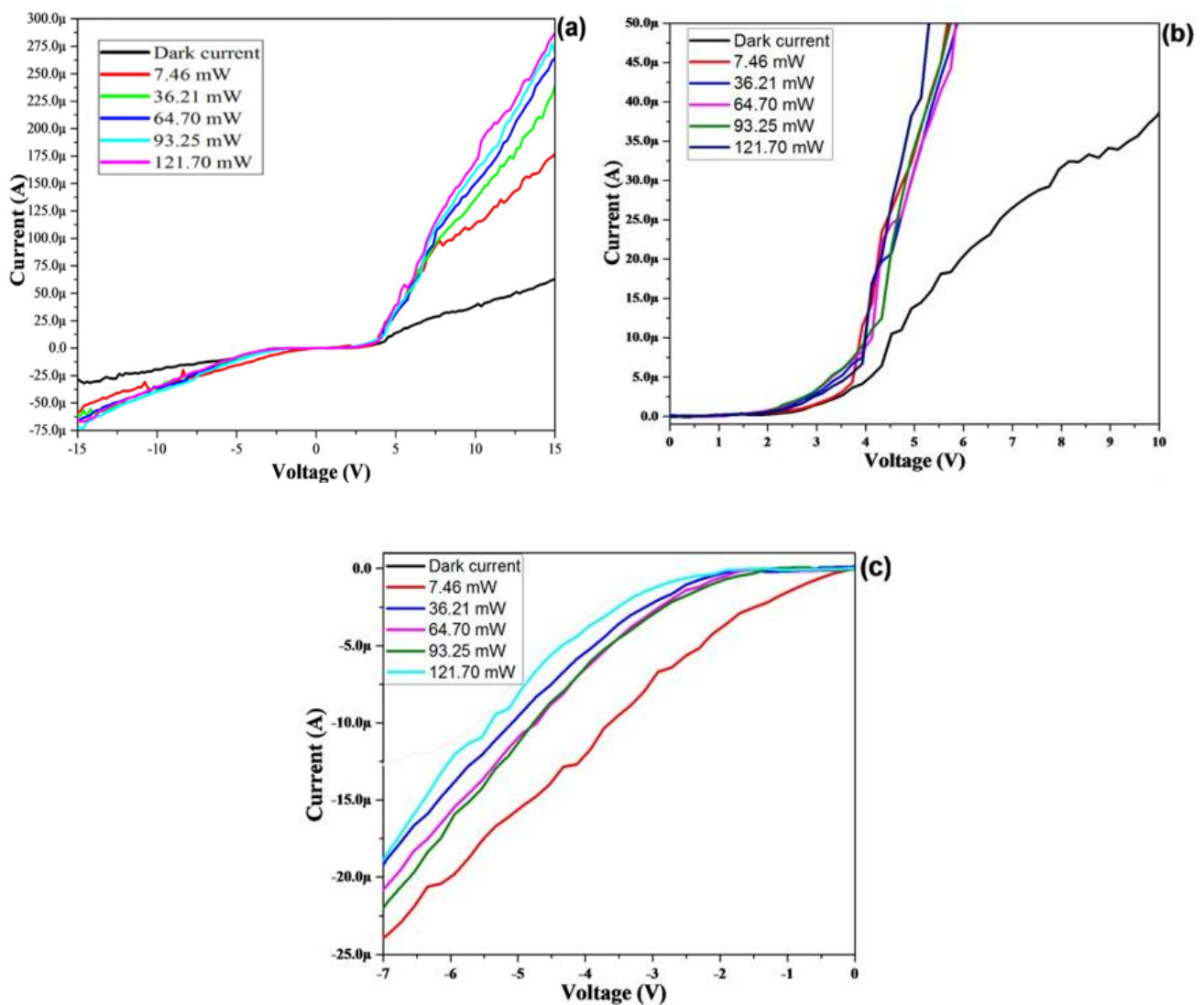


Fig. 4. (a) I-V characteristics of rGO photodetector under illumination by laser at 974 nm at various power, the insert, (b), shows enlarged version for DC bias voltage 0 to 10 V and (c) reverse bias voltage from 0 to -7 V (color online)

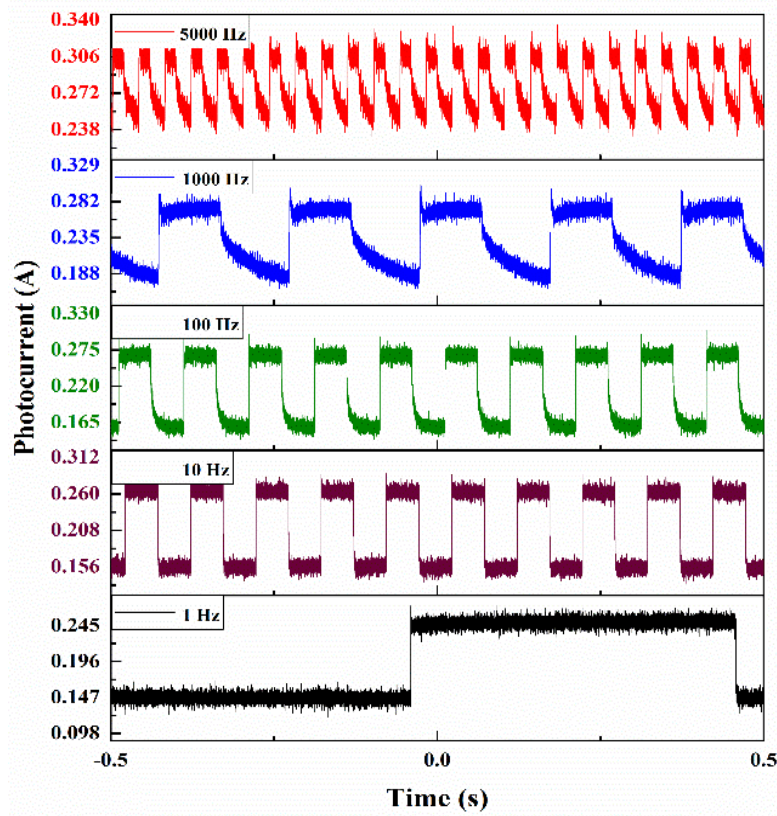


Fig. 5. rGO/p-Si photodetector showing the on and off pulse at frequency modulation of 1, 10, 100, 1000 and 5000 Hz (color online)

The I - V curves elucidate the dual characteristics of the IR rGO photodetector, which show positive and negative responses in the forward and reverse bias voltages, respectively, to laser illumination. Photoresponsivity (R_λ) is calculated by

$$R_\lambda = \frac{\Delta I}{P_i} \quad (1)$$

where ΔI is defined by $\Delta I = I_{ph} - I_{dc}$. I_{ph} is the generated photocurrent under laser illumination, I_{dc} is the dark current, and P_i is the optical power of the illuminating laser at 974 nm [47].

Table 1. Rise and fall time of sandwiched rGO/p-Si photodetector

Frequency (Hz)	Rise Time (μ s)	Fall Time (μ s)
1	11.97	712.33
10	11.72	640.97
100	7.77	548.49
1000	4.89	309.25
5000	4.01	96.28

Fig. 6 clearly shows that the photoresponsivity declines by increasing laser power in the forward bias region. The substantial characteristic of the fabricated IR rGO photodetector is the detection capability of IR illumination at 974 nm without any external power supply, which is at zero bias voltage. The built-in electric field causes the separation of photogenerated e - h pairs and at the same time leading to charge carrier recombination without contribution to the external photocurrent e - h pairs [48].

EQE is extracted from I - V curves, which is defined as the external quantum efficiency (EQE) that is the most important physical parameter determining the photo carrier collection efficiency and is expressed by [49 -51].

$$EQE = \frac{hc}{e\lambda} R_\lambda \quad (2)$$

where h is the Planck constant, e is the charge of an electron, R_λ is the photoresponsivity, c is the velocity of light, and λ is the wavelength of laser at 974 nm. Although the sensitivity of the rGO photodetector is low, high EQE of approximately 2% is obtained at the low laser power (7.64 mW) at DC bias of 15 V. Hence, the sufficient photon energy absorption and carrier recombination is due to the EQE having a value of more than 1, as noticeable in Fig. 6. An EQE value greater than 1 is achieved at DC bias greater than 7 V.

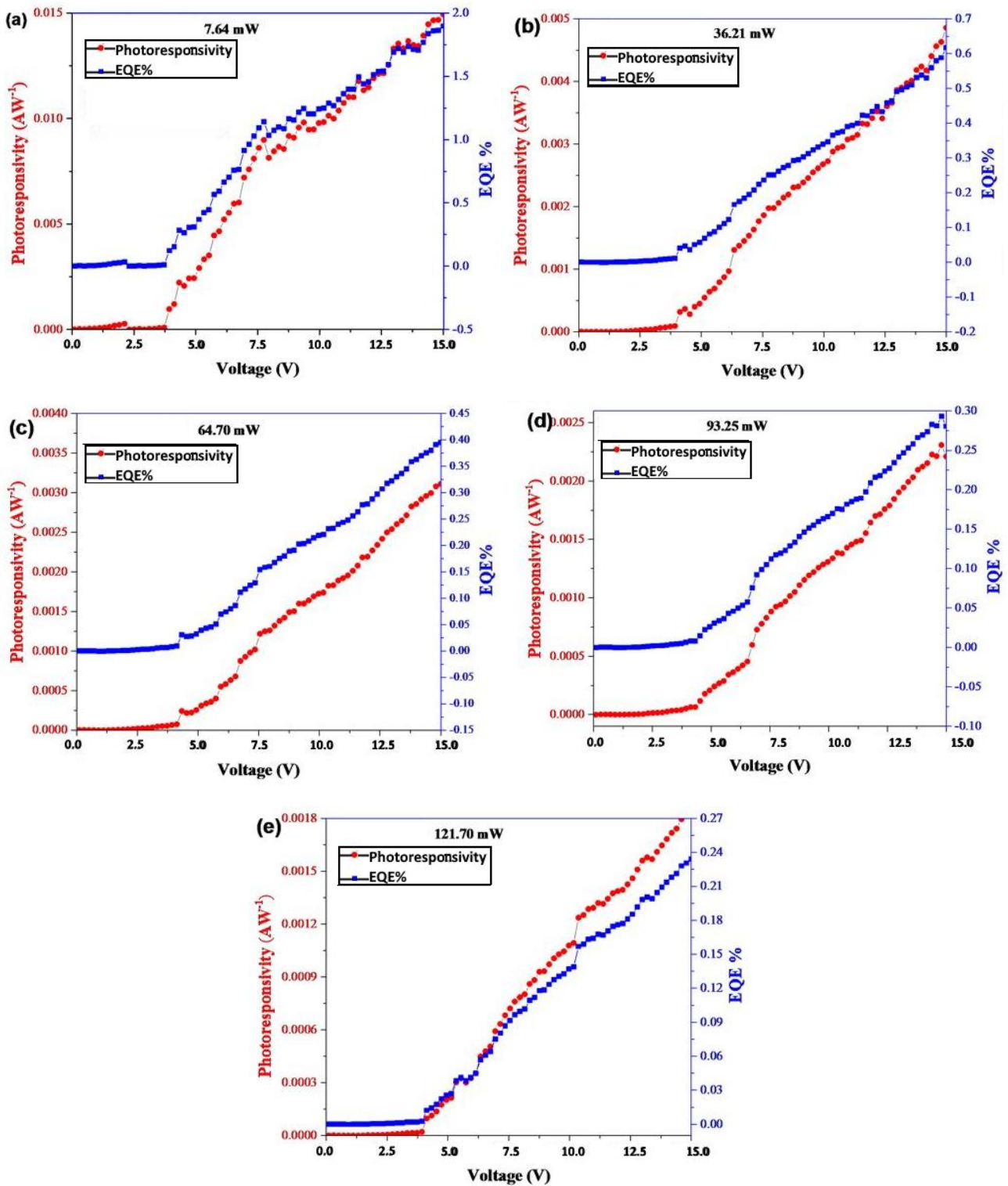


Fig. 6. Photoresponsivity (R_λ) and External Quantum Efficiency (EQE) of photodetector based on rGO under forward bias (a) 7.64 mW, (b) 36.21 mW, (c) 64.70, (d) 93.25 mW and (e) 121.70 mW (color online)

4. Conclusions

An IR photodetector containing two Ag electrodes was successfully fabricated by drop casting an rGO solution. The obtained results from SEM and EDX

confirmed excellent overlapping of few layers rGO on $\text{SiO}_2/\text{p-Si}$ substrate, which was further confirmed by the Raman scattering resulting D, G, 2D and S3 bands at 1345, 1577, 2674 and 2919 cm^{-1} respectively. The I - V characteristics indicated good Schottky contact at

increased laser power levels and DC bias voltage ranging from -15 to 15 V. The positive and negative photoresponsivity values of the photodetector for the forward and reverse DC bias voltages, respectively, confirmed the dual characteristics of the photodetector. The photoresponsivity and EQE values declined at increased LD power. A high EQE value of approximately 2% was obtained at 7.64 mW.

Acknowledgment

This work was supported by the University of Malaya [Grant Number RU 011 – 2019] and the Ministry of Higher Education, Malaysia [Grant Number HiCoE Phase II Funding]

References

- [1] K. S. Novoselov, A. Geim, *Nat. Mater.* **6**(3), 183 (2007).
- [2] H. Chang, H. Wu, *Energy Environ Sci.* **6**(12), 3483 (2013).
- [3] Y. Zhu, S. Murali, W. Cai, X. Li, J. W. Suk, J. R. Potts, R. S. Ruoff, *Adv Mater.* **22**(35), 3906 (2010).
- [4] C.-H. Liu, Y.-C. Chang, T. B. Norris, Z. Zhong, *Nat. Nanotechnol.* **9**(4), 273 (2014).
- [5] C. O. Kim, S. Kim, D. H. Shin, S. S. Kang, J. M. Kim, C. W. Jang, S. S. Joo, J. S. Lee, J. H. Kim, S.-H. Choi, *Nat. Commun.* **5**, 3249 (2014).
- [6] Y. Zhang, T. Liu, B. Meng, X. Li, G. Liang, X. Hu, Q. J. Wang, *Nat. Commun.* **4**, 1811 (2013).
- [7] X. Gan, R.-J. Shiue, Y. Gao, I. Meric, T. F. Heinz, K. Shepard, J. Hone, S. Assefa, D. Englund, *Nat. Photon.* **7**, 883 (2013).
- [8] F. Xia, T. Mueller, Y.-M. Lin, A. Valdes-Garcia, P. Avouris, *Nat. Nanotechnol.* **4**, 839 (2009).
- [9] R. R. Nair, P. Blake, A. N. Grigorenko, K. S. Novoselov, T. J. Booth, T. Stauber, N. M. Peres, A. K. Geim, *Science* **320**, 1308 (2008).
- [10] F. Wang, Y. Zhang, C. Tian, C. Girit, A. Zettl, M. Crommie, Y. R. Shen, *Sci.* **320**(5881), 206 (2008).
- [11] C. Xie, C. Mak, X. Tao, F. Yan, *Advanced Functional Materials* **27**(19), 1603886 (2017).
- [12] C. Xie, C. K. Liu, H. L. Loi, F. Yan, *Advanced Functional Materials* 1903907 (2019).
- [13] K. F. Mak, L. Ju, F. Wang, T. F. Heinz, *Solid State Commun.* **152**(15), 1341 (2012).
- [14] G. Eda, C. Mattevi, H. Yamaguchi, H. Kim, M. Chhowalla, *J. Phys. Chem. C* **113**(35), 15768 (2009).
- [15] Z. Wei, D. Wang, S. Kim, S.-Y. Kim, Y. Hu, M. K. Yakes, A. R. Laracuente, Z. Dai, S. R. Marder, C. Berger, *Sci.* **328**(5984), 1373 (2010).
- [16] S. Park, R. S. Ruoff, *Nat. Nanotechnol.* **4**, 217 (2009).
- [17] S. Stankovich, D. A. Dikin, G. H. Dommett, K. M. Kohlhaas, E. J. Zimney, E. A. Stach, R. D. Piner, S. T. Nguyen, R. S. Ruoff, *Nat.* **442**, 282 (2006).
- [18] C. Gómez-Navarro, J. C. Meyer, R. S. Sundaram, A. Chuvilin, S. Kurasch, M. Burghard, K. Kern, U. Kaiser, *Nano Lett.* **10**(4), 1144 (2010).
- [19] X. Wang, L. Zhi, K. Müllen, *Nano Lett.* **8**(1), 323 (2008).
- [20] D. Li, M. B. Müller, S. Gilje, R. B. Kaner, G. G. Wallace, *Nat. Nanotechnol.* **3**, 101 (2008).
- [21] G. Eda, G. Fanchini, M. Chhowalla, *Nat. Nanotechnol.* **3**, 270 (2008).
- [22] J. T. Robinson, F. K. Perkins, E. S. Snow, Z. Wei, P. E. Sheehan, *Nano Lett.* **8**(10), 3137 (2008).
- [23] X. Liu, L. Pan, T. Lv, G. Zhu, Z. Sun, C. Sun, *Chem. Commun.* **47**, 11984 (2011).
- [24] X. Liu, L. Pan, T. Lv, G. Zhu, T. Lu, Z. Sun, C. Sun, *RSC Adv.* **1**, 1245 (2011).
- [25] X. Liu, L. Pan, T. Lv, T. Lu, G. Zhu, Z. Sun, C. Sun, *Catal. Sci. Tech.* **1**, 1189 (2011).
- [26] B. Chitara, S. Krupanidhi, C. Rao, *Appl. Phys. Lett.* **99**(11), 113114 (2011).
- [27] B. Chitara, L. Panchakarla, S. Krupanidhi, C. Rao, *Adv. Mater.* **23**(45), 5419 (2011).
- [28] C.-K. Tseng, K.-H. Chen, W.-T. Chen, M.-C. M. Lee, N. Na, *IEEE Photon. Technol. Lett.* **26**(6), 591 (2014).
- [29] M. Zhang, D. Zhang, F. Jing, G. Liu, K. Lv, J. Zhou, S.-P. Ruan, *IEEE Photon. Technol. Lett.* **27**(1), 54 (2015).
- [30] H. Zhou, P. Gui, Q. Yu, J. Mei, H. Wang, G. Fang, *J. Mater. Chem. C* **3**, 990 (2015).
- [31] X. Li, H. Zhu, K. Wang, A. Cao, J. Wei, C. Li, Y. Jia, Z. Li, X. Li, D. Wu, *Adv. Mater.* **22**(25), 2743 (2010).
- [32] S. Darbari, V. Ahmadi, P. Afzali, Y. Abdi, M. Fedai, *J. Nanopart. Res.* **16**, 2798 (2014).
- [33] M. Zhang, D. Zhang, F. Jing, *IEEE Photon. Technol. Lett.* **28**(15), 1677 (2016).
- [34] G. E. Fernandes, J. H. Kim, D. Oller, J. Xu, *Appl. Phys. Lett.* **107**(11), 111111 (2015).
- [35] H. Chang, Z. Sun, M. Saito, Q. Yuan, H. Zhang, J. Li, Z. Wang, T. Fujita, F. Ding, Z. Zheng, *ACS Nano* **7**(7), 6310 (2013).
- [36] M. Acik, G. Lee, C. Mattevi, M. Chhowalla, K. Cho, Y. Chabal, *Nat. Mater.* **9**, 840 (2010).
- [37] G. Li, L. Liu, G. Wu, W. Chen, S. Qin, Y. Wang, T. Zhang, *Small* **12**(36), 5019 (2016).
- [38] J.-J. Zeng, Y.-J. Lin, *Appl. Phys. Lett.* **104**(13), 133506 (2014).
- [39] M. Rosli, P. Arasu, A. Noor, H. Lim, N. Huang, *J. Eur. Opt. Soc. Rapid. Publ.* **12**, 22 (2016).
- [40] R. Schönfelder, M. Rummeli, W. Gruner, M. Löffler, J. Acker, V. Hoffmann, T. Gemming, B. Büchner, T. Pichler, *Nanotechnol.* **18**(37), 375601 (2007).
- [41] F. T. Johra, J.-W. Lee, W.-G. Jung, *Ind. Eng. Chem. Res.* **20**(5), 2883 (2014).
- [42] K. Uchinokura, T. Sekine, E. Matsuura, *Solid State Communications* **11**, 47 (1972).
- [43] F. Vasko, V. Ryzhii, *Phys. Rev. B* **76**(1), 233404 (2007).
- [44] F. Rana, P. A. George, J. H. Strait, J. Dawlaty, S. Shivaraman, M. Chandrashekar, M. G. Spencer, *Phys. Rev. B* **79**, 115447 (2009).
- [45] E. J. Lee, K. Balasubramanian, R. T. Weitz, M.

- Burghard, K. Kern, *Nat. Nanotechnol.* **3**, 486 (2008).
- [46] W. Chen, F. Wang, S. Qin, J. Fang, C. Wang, G. Wang, L. Wang, X.-A. Zhang, *Appl. Phys. Lett.* **106**(2), 023122 (2015).
- [47] Y. Cao, J. Zhu, J. Xu, J. He, J. L. Sun, Y. Wang, Z. Zhao, *Small* **10**(12), 2345 (2014).
- [48] Z. Zhang, Q. Liao, Y. Yu, X. Wang, Y. Zhang, *Nano Energy* **9**, 237 (2014).
- [49] Q. Bao, H. Zhang, Z. Ni, Y. Wang, L. Polavarapu, Z. Shen, Q.-H. Xu, D. Tang, K. P. Loh, *Nano Res.* **4**(3), 297 (2011).
- [50] Y. Kim, D. H. Park, M. Du, W. L. Cao, C. H. Lee, W. N. Herman, D. B. Romero, in *Conference on Lasers and Electro-Optics*, Optical Society of America, (2007), CWH2, May 6; Baltimore, Maryland, United States.
- [51] C. Xie, Y. Wang, Z.-X. Zhang, D. Wang, L.-B. Luo, *Nano Today* **19**, 41 (2018).

*Corresponding author: harith@um.edu.my